arXiv:cond-mat/9608074v2 19 Aug 1996

Elastic scattering and absorption of surface acoustic waves by a quantum dot

Andreas Knäbchen and Yehoshua B. Levinson

Weizmann Institute of Science, Department of Condensed Matter Physics, 76100 Rehovot, Israel

Ora Entin-Wohlman

School of Physics and Astronomy, Raymond and Beverly Sackler Faculty of Exact Sciences, Tel Aviv University, 69978 Tel Aviv, Israel

(March 14, 2009)

Abstract

We study theoretically the piezoelectric interaction of a surface acoustic wave (SAW) with a two-dimensional electron gas confined to an isolated quantum dot. The electron motion in the dot is diffusive. The electron-electron interaction is accounted for by solving the screening problem in real space. Since the screening in GaAs/Al_xGa_{1-x}As heterostructures is strong, an approximate inversion of the dielectric function $\epsilon(\boldsymbol{r},\boldsymbol{r}')$ can be utilized, providing a comprehensive qualitative picture of the screened SAW potential and the charge redistribution in the dot. We calculate the absorption and the scattering cross-sections for SAW's as a function of the area of the dot, A, the sound wave vector, q, and the diffusion coefficient D of the electrons. Approximate analytical expressions for the cross-sections are derived for all cases where the quantities q^2A and $A\omega/D$ are much larger or smaller than unity; ω is the SAW frequency. Numerical results which include the intermediate regimes and show the sample-specific dependence of the cross-sections on the angles

of incidence and scattering of surface phonons are discussed. The weak localization corrections to the cross-sections are found and discussed as a function of a weak magnetic field, the frequency, and the temperature. Due to the absence of current-carrying contacts, the phase coherence of the electron motion, and in turn the quantum corrections, increase as the size of the dot shrinks. This shows that scattering and absorption of sound as noninvasive probes may be advantageous in comparison to transport experiments for the investigation of very small electronic systems.
PACS: 72.50, 73.35, 72.15R

Typeset using REVTEX

I. INTRODUCTION

During the last decade, a number of theoretical papers which address the application of ultrasound for the investigation of quantum effects in disordered electronic systems has been published. Mainly quantum corrections to the sound absorption in infinite systems have been studied. For instance, the contribution of weak localization effects to the absorption coefficient has been calculated in Refs.[1–5]. Electron-electron interaction effects have been addressed in Refs.[1] and[2]. A particularly detailed discussion of these effects, including both the diffusion and the cooper channel terms, is given in Ref.[5]. The interaction of sound with electrons confined to a finite mesoscopic system has only been studied with respect to the fluctuations of the ultrasound absorption.[6,7] The main idea of these two works is that the ultrasound absorption is a noninvasive probe which can be used to investigate isolated metallic samples [no leads attached]. In all these works, the calculations have essentially been done for the deformation potential interaction of bulk phonons with three-dimensional [3D] electron systems. To ensure an efficient coupling to the 3D phonon wave, the dimensionality of the electron system cannot be reduced, though this is necessary in order to enhance the weak localization effects. To overcome the restrictions associated with bulk phonons, we propose to consider the interaction of surface acoustic waves[8,9] (SAW's) with 2D electron systems.[10] This interaction is very strong in GaAs/$Al_xGa_{1-x}As$ heterostructures where it is caused by the piezoelectric field accompanying the SAW. Indeed, the SAW technique has been used successfully to investigate both the integer and the fractional quantum Hall regime.[11–15] These experiments have shown, e.g., that the SAW technique is suited to resolve very small spatial inhomogeneities in the areal electron density which are not visible in dc magnetoresistance measurements.[12,15] Effects of electron heating due to the electric field accompanying the SAW have been discussed in Refs.[11] and[12]. Though the absorption of SAW's in these experiments is used to study extended electron systems, the SAW technique might be applied to mesoscopic systems as well. In this case, the noninvasive character of such a measurement could prove advantageous. In a very recent experiment,[16] the direct

acousto-electric current induced by a SAW through a *single* quantum point contact has been observed. The length of the quasi-one-dimensional channel [which determines the size of the interaction region] was about 0.5 μm.

It is the main purpose of this paper to consider theoretically some of the effects associated with a noninvasive probing of mesoscopic 2D electron systems by SAW's. Specifically, we address the scattering and absorption of SAW's due to the electrons confined to an isolated quantum dot, see Fig. 1. One of the main quantities to be calculated in this framework is the elastic differential scattering cross-section $\eta_{sc}(\boldsymbol{q'}, \boldsymbol{q})$. By definition, $\eta_{sc} d\varphi$ is the ratio of the sound intensity flux scattered into a "solid" angle $d\varphi$ around $\boldsymbol{q'}$ and the flux intensity I of the incoming surface wave with wave vector $\boldsymbol{q}$, $q = q'$. Besides η_{sc}, we introduce the cross-section η_{abs} characterizing the phonon absorption. [Though η_{sc} and η_{abs} have the dimension of a length in two dimensions, we shall use the familiar term cross-section.] $I\eta_{abs}$ gives the energy per unit time absorbed by the electrons in the dot from the acoustic wave field. Hence, this quantity is directly associated with electron heating.

We calculate the weak localization corrections to both η_{sc} and η_{abs}. Since the sample is isolated, the phase coherence is not reduced by leads which are necessarily attached to the dot in an electron transport measurement. This in turn affects the magnitude of the weak localization corrections and their dependence on the size of the dot. Though weak localization effects contribute only correction terms to the classical cross-sections, their dependence on weak magnetic fields and the phase coherence time (i.e. the temperature) can be used to detect them. Their particular dependence on the frequency is superimposed on that of the classical components of η_{sc} and η_{abs} and might therefore be difficult to resolve.

The screening of the electron-phonon coupling arises from the electrons confined to the dot and is not a negligible effect. We account for the screening in the linear response approximation, where the change of the electron density arising from the external perturbation is proportional to the magnitude of the perturbation. This approach is justified by the small SAW intensities used in experiments. Since we consider a system without translational invariance, the equations for the screened potential, the charge redistribution, etc. have to be

formulated in real space. Consequently, screening cannot be taken into account by simply multiplying the unscreened potential by a dielectric function $\epsilon(\omega, \boldsymbol{q})$ but involves the inversion of the dielectric function (or matrix) $\epsilon(\boldsymbol{r}, \boldsymbol{r}')$. To do this accurately, i.e. to account for the shape of the dot and the direction of the incoming SAW, we have performed numerical calculations. Analytically, one can exploit the fact that the screening is strong. In particular, for wavelengths $2\pi/q$ which are larger than the size L of the dot, a series expansion of ϵ^{-1} in terms of the small parameter a_B/L can be utilized, where a_B is the effective Bohr radius. This provides a rather complete qualitative understanding of the relations between the bare and the screened SAW potential and the charge redistribution in the dot.

In the calculation of the cross-sections η_{sc} and η_{abs} we mainly focus on the cases where qL is of the order of or smaller than unity. The quantum dot will be considered in the diffusive limit, i.e. the size L of the dot is large compared to the elastic mean free path l. In addition, l has to be small compared to the wavelength $2\pi/q$ of the SAW, $ql \ll 1$. This relation guarantees $\omega\tau \ll 1$, because the velocity of sound, $s = \omega/q$, is much smaller than the Fermi velocity, $v_F = l/\tau$. From an experimental point of view, these conditions are satisfied in a dot of size $L \simeq 1$ μm, patterened in an electron gas with a low mobility ($\mu \simeq 10^4$ cm^2/Vs) corresponding to $l \simeq 100$ nm. So, except for the shortest SAW's used in recent experiments,[12–15,10,16] ql is indeed small.

This paper is organized in the following way. In Sec. II, we summarize the main equations for the scattering and the absorption cross-sections, the bare SAW potential arising from the piezoelectric coupling, and the dielectric function. The cross-sections η_{sc} and η_{abs} and, within the linear screening approach, the dielectric function $\epsilon(\boldsymbol{r}, \boldsymbol{r}')$ are essentially determined by the density-density correlator $\Pi_\omega(\boldsymbol{r}, \boldsymbol{r}')$. This quantity is specified in Sec. III for the case of a diffusive system, where it comprises besides the classical term weak localization corrections. Based on these results, we discuss $\epsilon(\boldsymbol{r}, \boldsymbol{r}')$ and its appropriate matrix representation in Sec. IV. An approximate inversion of ϵ is carried out analytically in the strong screening regime. This yields the screened potential in the dot in terms of the bare SAW field. Combining these results with the equations for $\Pi_\omega(\boldsymbol{r}, \boldsymbol{r}')$, we evaluate the cross-sections in the limiting

cases $qL \ll 1$ and $qL \gg 1$ in Sec. V. The weak localization corrections to η_{sc} and η_{abs} are related to the cooperon $\mathcal{C}_\omega(\boldsymbol{r}, \boldsymbol{r})$. Its equation is solved in Sec. VI. Special emphasis is put on the dependence of $\mathcal{C}_\omega(\boldsymbol{r}, \boldsymbol{r})$ on the magnetic field. Results of a numerical computation of the scattering and the absorption cross-sections are presented in Sec. VII. Conclusions are given in the last section.

II. BASIC EQUATIONS

The interaction between the SAW and the electrons in the quantum dot gives rise to finite probabilities for the absorption and the scattering of phonons. A Golden Rule calculation can be used to obtain the corresponding cross-sections. The amplitude for the absorption of a phonon results from a first-order process between the (phonon) states $|\boldsymbol{q}\rangle$ and $|0\rangle$, see Fig. 2; $\boldsymbol{q}$ is the 2D phonon wave vector. Scattering is a second-order process involving the two intermediate states $|\boldsymbol{q}, \boldsymbol{q}'\rangle$ and $|0, 0\rangle$ with two or no phonons, depending on whether the emission of the second phonon occurs before or after the absorption of the incoming one. The absorption and (elastic) scattering cross-sections have the form (a factor of 2 accounting for the spin degeneracy is included)

$$\eta_{abs}(\boldsymbol{q}) = -\frac{4\mathcal{L}^2}{s\hbar}\Im[\Pi_\omega(\boldsymbol{q}, \boldsymbol{q})], \tag{1}$$

and

$$\eta_{sc}(\boldsymbol{q'}, \boldsymbol{q}) = \frac{q\mathcal{L}^4}{\pi s^2\hbar^2}|\Pi_\omega(\boldsymbol{q'}, \boldsymbol{q})|^2, \tag{2}$$

where s is the velocity of surface sound and

$$\Pi_\omega(\boldsymbol{q}, \boldsymbol{q}') \equiv \int d^3\boldsymbol{R} \int d^3\boldsymbol{R}'\, V^*_{\boldsymbol{q}}(\boldsymbol{R})\Pi_\omega(\boldsymbol{R}, \boldsymbol{R}')V_{\boldsymbol{q}'}(\boldsymbol{R}'). \tag{3}$$

Here, $\boldsymbol{R}$ is a 3D real space vector and $V_{\boldsymbol{q}}$ denotes the *screened* potential associated with one surface phonon with wave vector $\boldsymbol{q}$ in the normalization area $\mathcal{L}^2$. The quantity $\mathcal{L}$ does not enter the final results since it is canceled by corresponding terms originating form the

SAW potential, see Eq. (8) below. The retarded density-density correlator $\Pi_\omega(\boldsymbol{R}, \boldsymbol{R'})$ of the electrons in the dot is defined by[17]

$$\Pi_\omega(\boldsymbol{R}, \boldsymbol{R'}) = -(i/\hbar) \int_0^\infty dt\, e^{i\omega t} \left\langle [\rho(\boldsymbol{R}, t), \rho(\boldsymbol{R'}, 0)] \right\rangle , \tag{4}$$

where $\rho(\boldsymbol{R}, t)$ is the electron density operator for one spin component and $\omega = qs$ is the SAW frequency.

Equation (3) can be simplified by making use of the fact that the thickness of the 2D electron gas (2DEG) is much smaller than the penetration depth of the SAW into the interior of the sample. This allows one to neglect the finite extend of the 2DEG in the z-direction, replacing $\rho(\boldsymbol{R}, t)$ by $\delta(z - d)\rho(\boldsymbol{r}, t)$, where d is the distance between the 2DEG and the surface of the sample and $\rho(\boldsymbol{r}, t)$ is the areal density of 2D electrons. [We have $\boldsymbol{R} = (\boldsymbol{r}, z)$ where $\boldsymbol{r}$ is a vector in the plane of the 2DEG and z is the co-ordinate perpendicular to it; see Fig. 1.] Substituting this replacement into Eq. (4) yields

$$\Pi_\omega(\boldsymbol{R}, \boldsymbol{R}') = \delta(z - d)\delta(z' - d)\Pi_\omega(\boldsymbol{r}, \boldsymbol{r}'), \tag{5}$$

where $\Pi_\omega(\boldsymbol{r}, \boldsymbol{r}')$ is the remaining 2D density-density correlator. Particle number conservation can be expressed in terms of $\Pi_\omega(\boldsymbol{r}, \boldsymbol{r}')$ in the form

$$\int d^2\boldsymbol{r}\, \Pi_\omega(\boldsymbol{r}, \boldsymbol{r}') = \int d^2\boldsymbol{r}'\, \Pi_\omega(\boldsymbol{r}, \boldsymbol{r}') = 0. \tag{6}$$

Substituting Eq. (5) into Eq. (3), we obtain

$$\Pi_\omega(\boldsymbol{q}, \boldsymbol{q}') \equiv \int d^2\boldsymbol{r} \int d^2\boldsymbol{r}'\, V^*_{\boldsymbol{q}}(\boldsymbol{r}, z = d)\Pi_\omega(\boldsymbol{r}, \boldsymbol{r}')V_{\boldsymbol{q}'}(\boldsymbol{r}', z' = d). \tag{7}$$

The integrations run over the area A of the dot.

The bare potential V^{ph} created by the SAW in the plane of the 2DEG can be represented in the form[18]

$$V^{ph}_{\boldsymbol{q}}(\boldsymbol{r}, z = d) = \frac{1}{\mathcal{L}}\gamma_{\boldsymbol{q}} e^{i\boldsymbol{q}\boldsymbol{r}}. \tag{8}$$

For GaAs/Al_xGa_{1-x}As heterostructures and the range of wavelengths used in SAW experiments, the piezoelectric electron-phonon interaction is dominant. We may thus identify

$\gamma_{\boldsymbol{q}}$ with the piezoelectric vertex $\gamma_{\boldsymbol{q}}^{PA}$, neglecting the deformation potential coupling. In addition, since qd is usually much smaller than unity, the dependence of $\gamma_{\boldsymbol{q}}^{PA}$ on d can be disregarded. [For $qd \sim 1$, $\gamma_{\boldsymbol{q}}$ depends non-monotonously on the parameter qd, see the discussion in Ref.[19].] Then, we have

$$\gamma_{\boldsymbol{q}} = \gamma_{\boldsymbol{q}}^{PA} = (\hbar/\rho s a_{PA})^{1/2} \beta e \hat{q}_x \hat{q}_y = 3.7 \hat{q}_x \hat{q}_y 10^{-10} \text{ eVcm}, \tag{9}$$

where ρ is the mass density of the lattice, e is the electron charge, and a_{PA} represents a numerical factor which can be expressed in terms of the elastic constants of the lattice, cf. Ref.[18]. Equation (9) is valid for a GaAs-type crystal with the SAW propagating along the (100) plane and electrically free[8] boundary conditions for the piezoelectric potential at the surface. In this case all (non-zero) piezoelectric moduli are equal to β. $\hat{q}_x$ (and, similarly, $\hat{q}_y$) is the component of $\hat{\boldsymbol{q}}$ in the direction of the lattice axis x on the surface. The numerical value given on the right-hand-side of Eq. (9) applies to GaAs/Al_xGa_{1-x}As heterostructures.

The potential V^{ph} associated with the SAW acts on the electrons in the dot and leads to their redistribution. This creates a potential V^{ch} which adds to V^{ph}. The resulting total potential

$$V = V^{ch} + V^{ph} \tag{10}$$

is the relevant quantity which determines the absorption and the scattering of surface phonons by the quantum dot; see Eq. (3). The calculation of the total potential V and the corresponding charge redistribution $\delta\rho(\boldsymbol{r})$ has to be done self-consistently. Although the electron distribution has been restricted to a plane, the electrostatic problem is still a three-dimensional one. Bearing in mind that the quantum dot is embedded in a semiconductor with dielectric constant $\epsilon_\circ$, we can write the following equations[17]

$$\delta\rho(\boldsymbol{r}) = 2 \int d^2\boldsymbol{r}' \, \Pi_\omega(\boldsymbol{r}, \boldsymbol{r}') V(\boldsymbol{r}', z' = d), \tag{11}$$

$$\nabla^2 V^{ch}(\boldsymbol{R}) = -\frac{4\pi e^2}{\epsilon_\circ} \delta(z - d) \delta\rho(\boldsymbol{r}), \tag{12}$$

where the factor of 2 is due to spin degeneracy and it is understood that all potentials and $\delta\rho(\boldsymbol{r})$ refer to the ω-component in the corresponding Fourier expansions. Note that Eqs. (10)–(12) reduce for a translational invariant system to the well-known Random Phase Approximation for the dielectric function.

The solution of Poisson's equation (12) can be expressed in terms of the corresponding Green's function

$$\nabla^2 G(\boldsymbol{R}, \boldsymbol{R}') = -4\pi\delta(\boldsymbol{R} - \boldsymbol{R}') \tag{13}$$

which has to satisfy the boundary conditions at the interface between the sample and the halfspace (dielectric constant ϵ_1) above it. (The SAW potential V^{ph} satisfies the boundary conditions so that the total potential V meets all requirements provided that V^{ch} does.) Addressing the case where both $\boldsymbol{R}$ and $\boldsymbol{R}'$ lie in the plane of the dot ($z = z' = d$), we have[20]

$$G(\boldsymbol{R}, \boldsymbol{R}') = G(\boldsymbol{r} - \boldsymbol{r}') = \frac{1}{|\boldsymbol{r} - \boldsymbol{r}'|} + \frac{\epsilon_\circ - \epsilon_1}{\epsilon_\circ + \epsilon_1} \frac{1}{\sqrt{|\boldsymbol{r} - \boldsymbol{r}'|^2 + (2d)^2}}. \tag{14}$$

The Green's function G can be combined with Eqs. (10)–(12) to relate the total potential directly to the SAW field

$$\int d^2\boldsymbol{r}'\, \epsilon(\boldsymbol{r}, \boldsymbol{r}') V(\boldsymbol{r}', z' = d) = V^{ph}(\boldsymbol{r}, z = d). \tag{15}$$

The kernel of this integral equation is the dielectric function

$$\epsilon(\boldsymbol{r}, \boldsymbol{r}') = \delta(\boldsymbol{r} - \boldsymbol{r}') - 2\frac{e^2}{\epsilon_\circ} \int d^2\boldsymbol{r}''\, G(\boldsymbol{r} - \boldsymbol{r}'') \Pi_\omega(\boldsymbol{r}'', \boldsymbol{r}'). \tag{16}$$

Using Eq. (6), one can see that $\int d^2\boldsymbol{r}'\, \epsilon(\boldsymbol{r}, \boldsymbol{r}') = 1$. This means that a potential which is spatially constant within the dot is not screened, cf. Eq. (15).

III. DENSITY-DENSITY CORRELATOR FOR A DIFFUSIVE SYSTEM

In the diffusive regime, the density-density correlator[21] has the form

$$\Pi_\omega(\boldsymbol{r}, \boldsymbol{r}') = -\nu \left[\delta(\boldsymbol{r} - \boldsymbol{r}') + i\omega \mathcal{D}_\omega(\boldsymbol{r}, \boldsymbol{r}')\right], \tag{17}$$

where $\mathcal{D}_\omega$ is the diffusion propagator and ν is the (2D) density of states for one spin projection. This result is valid for small frequencies $\omega\tau \ll 1$, small wave vectors $ql \ll 1$, and low temperatures $\omega, T \ll \epsilon_F$; τ and l denote the elastic mean free time and mean free path, respectively, and ϵ_F is the Fermi energy. q describes the spatial modulation of an external potential, the response to which can be expressed in terms of Π_ω, Eq. (17). In our case, q is the wave number of the SAW's. Neglecting weak localization corrections, the diffusion propagator satisfies in real space the equation[21]

$$[-i\omega - D\nabla^2]\mathcal{D}_\omega(\boldsymbol{r}, \boldsymbol{r'}) = \delta(\boldsymbol{r} - \boldsymbol{r'}) \qquad \nabla_n \mathcal{D}_\omega|_b = 0, \tag{18}$$

where $D = l^2/2\tau$ is the 2D diffusion coefficient and the outer normal component of a vector [here the gradient] with respect to the boundary of the quantum dot is denoted by a subscript n. The boundary condition follows from the requirement that there is no flow of electrons through the boundary of the system. This is in contrast to a system coupled to leads, where the particle density is fixed in the contact regions, i.e. $\mathcal{D}|_c = 0$.

The diffusion propagator, Eq. (18), can be expressed in terms of its eigenfunctions as follows

$$\mathcal{D}_\omega(\boldsymbol{r}, \boldsymbol{r'}) = \sum_{m=0}^{\infty} \frac{\psi_m(\boldsymbol{r})\psi_m(\boldsymbol{r'})}{-i\omega + D\lambda_m}. \tag{19}$$

The diffusion modes are defined by

$$[\nabla^2 + \lambda_m]\psi_m(\boldsymbol{r}) = 0, \qquad \nabla_n \psi_m|_b = 0. \tag{20}$$

They are orthogonal to each other and are normalized, $\int d^2\boldsymbol{r}\, \psi_m \psi_n = \delta_{m,n}$. It is a peculiar feature of an isolated quantum dot that there exists a zeroth eigenfunction $\psi_0 = 1/\sqrt{A}$, A being the area of the dot. The corresponding eigenvalue $\lambda_0 = 0$ is well separated from the remaining sequence of eigenvalues $\lambda_m \sim A^{-1}$. The zeroth mode determines the behavior of the diffusion propagator in the case of a "small" dot, $A\omega/D \ll 1$. In this regime, the particle is able to diffuse through the whole system within one period of the external potential. Boundary effects are crucial and we obtain from Eq. (19) $\mathcal{D}_\omega(\boldsymbol{r}, \boldsymbol{r'}) \simeq (-i\omega A)^{-1}$. In the opposite,

"big-dot" case, $A\omega/D \gg 1$, the particle diffuses only over a distance $\sqrt{D/\omega} \ll \sqrt{A}$ before the external potential is reversed. Thus, the diffusion process is bulk-like. Disregarding all boundary effects, Eq. (19) reduces in this case to the translational invariant form $\mathcal{D}_\omega(\boldsymbol{r}-\boldsymbol{r'})$, corresponding to an infinitely extended system. In the intermediate regime, $A\omega/D \simeq 1$, the diffusion propagator exhibits sample-specific properties.

Weak localization effects yield a correction term δD to the classical diffusion coefficient D which basically describes the slowing down of the diffusion processes due to enhanced backscattering.[21,22] Generally, δD may depend on the frequency ω, the electron phase coherence time τ_ϕ, a weak magnetic field B, and other physical parameters. In addition to this, the weak localization correction to D acquires in a finite system a spatial dependence. To account for a spatially varying diffusion coefficient in Eq. (18) for the diffusion propagator, we use the replacement[22]

$$D\nabla^2 \longrightarrow \nabla(D + \delta D(\boldsymbol{r}))\nabla. \tag{21}$$

where all other variables of δD are suppressed. This replacement guarantees particle number conservation. Since we are only interested in the first order corrections due to $\delta D(\boldsymbol{r})$, we write the diffusion propagator in the from $\mathcal{D}_\omega + \delta\mathcal{D}_\omega$. Substituting this ansatz in the modified Eq. (18) yields

$$\delta\mathcal{D}_\omega(\boldsymbol{r},\boldsymbol{r'}) = \int d^2\boldsymbol{r''}\, \mathcal{D}_\omega(\boldsymbol{r},\boldsymbol{r''})\{\nabla''\delta D(\boldsymbol{r''})\nabla''\}\mathcal{D}_\omega(\boldsymbol{r''},\boldsymbol{r'}). \tag{22}$$

Neglecting spin scattering, the weak localization correction to the diffusion coefficient can be expressed in terms of the cooperon[22,21] $\mathcal{C}$ as follows

$$\delta D(\boldsymbol{r}) = -\frac{D}{\pi\hbar\nu}\mathcal{C}_\omega(\boldsymbol{r},\boldsymbol{r}). \tag{23}$$

In real space, the cooperon obeys the equation[21]

$$[-i\omega + \tau_\phi^{-1} + D(i\nabla + (2e/c\hbar)\boldsymbol{A}(\boldsymbol{r}))^2]\mathcal{C}_\omega(\boldsymbol{r},\boldsymbol{r'}) = \delta(\boldsymbol{r}-\boldsymbol{r'}) \tag{24}$$

$$(i\nabla_n + (2e/c\hbar)\boldsymbol{A}_n(\boldsymbol{r}))\mathcal{C}_\omega|_b = 0.$$

The influence of a (weak) magnetic field $\boldsymbol{B}$ is described by the vector potential $\boldsymbol{A}(\boldsymbol{r})$. The field $\boldsymbol{B}$ is oriented perpendicularly to the plane of the 2DEG. The boundary condition in Eq. (24) ensures that there is no flow of "coherence" ($\mathcal{C}$) through the boundary of an isolated system. In contrast, the phase randomization provided by a massive contact is described by $\mathcal{C}|_c = 0$. Here, we do not proceed with the evaluation of the cooperon; this will be done in Sec. VI. For the rest of this and the next two sections it will be sufficient to bear in mind that $\delta D(\boldsymbol{r})$ is a well-defined quantity which can be calculated according to Eq. (23).

Let us now return to the density-density correlator. Substituting Eqs. (19) and (22) into Eq. (17) yields Π_ω in terms of the diffusion modes in the form

$$\Pi_\omega(\boldsymbol{r}, \boldsymbol{r}') = -\nu \sum_{m,n=1}^{\infty} \beta_{mn} \psi_m(\boldsymbol{r}) \psi_n(\boldsymbol{r}'), \tag{25}$$

where

$$\beta_{mn} = \beta_m \delta_{m,n} + \delta\beta_{mn} \tag{26}$$

is decomposed into the classical term

$$\beta_m = \frac{D\lambda_m}{-i\omega + D\lambda_m} \tag{27}$$

and the weak localization contribution

$$\delta\beta_{mn} = \frac{-i\omega}{(-i\omega + D\lambda_m)(-i\omega + D\lambda_n)} \int d^2\boldsymbol{r}\, \delta D(\boldsymbol{r}) \nabla\psi_m(\boldsymbol{r}) \nabla\psi_n(\boldsymbol{r}). \tag{28}$$

The sums over modes in Eq. (25) start from $m, n = 1$ since $\beta_{m0} = \beta_{0m} = 0$ for $m = 0, 1, \ldots$. It can easily be seen that this is a consequence of the structure of the diffusion propagator [Eqs. (18) and (21)] and holds true even for the case where $\delta D(\boldsymbol{r})$ is treated exactly (i.e. not only to first order). The restriction of the summations means that, while the zeroth mode contributes to the diffusion propagator, it does not influence the density-density correlator. The latter fulfills Eqs. (6) because $\int d^2\boldsymbol{r}\, \psi_m = 0$ for $m \geq 1$.

IV. SCREENING

In order to apply Eq. (15), the relation between the bare SAW field and the screened potential V, to the diffusive dot under consideration, we consider its representation in terms of the diffusion modes defined in Eq. (20). The matrix elements of the density-density correlator are given in Eq. (25), while those of the Green's function G [Eq. (14)] can be written as

$$G_{mn} = \int d^2\boldsymbol{r}' \int d^2\boldsymbol{r}\, \psi_m(\boldsymbol{r}) G(\boldsymbol{r}-\boldsymbol{r}')\psi_n(\boldsymbol{r}'). \tag{29}$$

For the potential V (and, similarly, for V^{ph}), we introduce the expansion

$$V(\boldsymbol{r}, z=d) = \sum_{n=0}^{\infty} V_n \psi_n(\boldsymbol{r}), \qquad V_n = \int d^2\boldsymbol{r}\, \psi_n(\boldsymbol{r}) V(\boldsymbol{r}, z=d). \tag{30}$$

Using these definitions, the complete set of equations which follows from Eq. (15) can be written in the form

$$V_0^{ph} = V_0 + 2\frac{e^2\nu}{\epsilon_\circ} \sum_{n,l\geq 1} G_{0l}\beta_{ln} V_n, \tag{31}$$

$$V_m^{ph} = V_m + 2\frac{e^2\nu}{\epsilon_\circ} \sum_{n,l\geq 1} G_{ml}\beta_{ln} V_n\,, \quad m \geq 1. \tag{32}$$

These equations have to be solved with respect to $\{V_n\}$. Not all of these quantities are coupled to each other. For example, as emphasized by Eqs. (31) and (32), the $\{V_n\}$, $n \geq 1$, form a closed system of equations. Its solution can be substituted into Eq. (31) determining the element V_0. This property of the screening equations results from the fact that, due to charge conservation, $\beta_{l0} = 0$, cf. the discussion after Eq. (28).

The formal solution of Eq. (32) can be given in terms of an inverse dielectric matrix $[m \geq 1]$

$$V_m = \sum_{n\geq 1} (\epsilon^{-1})_{mn} V_n^{ph}. \tag{33}$$

A precise calculation of the elements $(\epsilon^{-1})_{mn}$ has to be done numerically. This is described in Sec. VII. Here, we shall exploit the following facts. First, the SAW potential is slowly varying

on the scale of the dot. Indeed, for usual sound frequencies, V^{ph} oscillates once or a few times across the dot. Consequently, only the first few elements V_n^{ph} are significantly different from zero. With respect to the matrices G_{mn}, β_{mn}, and $(\epsilon^{-1})_{mn}$, we may also concentrate on the indices m and n which are of order unity. Secondly, the screening in experimentally relevant samples is strong. To see this, we estimate the magnitude of the different terms in Eqs. (31) and (32). Using $\nu = m^*/2\pi\hbar^2$, the prefactor $2e^2\nu/\epsilon_\circ$ can be written in the form $1/\pi a_B$, where $a_B = \epsilon_\circ/e^2 m^*$ is the effective Bohr radius of the lattice and m^* is the effective electron mass. Since $a_B = 10.6$ nm for GaAs, the Bohr radius represents the smallest length scale in the system. The matrix element G_{mn} is of order $1/\sqrt{\lambda_m} \simeq L/m$ for $m \approx n$, $L \equiv \sqrt{A}$ being the size of the dot, and it decreases sharply for m or n much larger than unity and very different from each other. Hence, we have $(2e^2\nu/\epsilon_\circ)G_{mn} \simeq L/a_B$ for the relevant m and n of order unity. We therefore expect V_m to be of order $(a_B/L)V_m^{ph} \ll V_m^{ph}$.

An approximate inversion of Eq. (32) providing the leading terms in an expansion with respect to a_B/L can be accomplished by introducing the inverse matrix $(G^{-1})_{ml}$ to the reduced matrix G_{ml} with indices m and l equal to or larger than unity. Similarly, we define $(\beta^{-1})_{ml}$. Multiplying Eq. (32) with $\beta^{-1}G^{-1}$ yields for the inverse dielectric operator [Eq. (33)]

$$(\epsilon^{-1})_{mn} = \frac{\pi a_B}{L} \sum_{l\geq 1} (\beta^{-1})_{ml} (\tilde{G}^{-1})_{ln} + \mathcal{O}(a_B^2/L^2), \tag{34}$$

where $\tilde{G} \equiv G/L$ is a dimensionless Green's function depending only on the shape of the dot.

Substituting Eqs. (34) and (33) into Eq. (31), we obtain for the $\boldsymbol{r}$-independent part of the total potential

$$V_0 = V_0^{ph} - \sum_{n,l\geq 1} G_{0l} (G^{-1})_{ln} V_n^{ph} + \mathcal{O}(a_B/L). \tag{35}$$

This equation confirms explicitly the conclusion following from the general Eq. (16), namely that the spatially uniform part of an external potential, here V_0^{ph}, contributes unscreened to V_0. Moreover, since the product GG^{-1} is of order unity, it shows that also the spatially varying components V_n^{ph} contribute effectively unscreened to V_0. Combining Eqs. (34) and (35), we find for the total potential

$$V(\boldsymbol{r}) \approx \frac{1}{\sqrt{A}} V_0 + \frac{\pi a_B}{L} \sum_{m,n,l\geq 1} \psi_m(\boldsymbol{r}) (\beta^{-1})_{mn} (\tilde{G}^{-1})_{nl} V_l^{ph}. \tag{36}$$

This result shows that, in contrast to an open or an infinitely extended system, the case of strong screening in an isolated dot is characterized by small variations of the total potential (the second term) existing on top of a large but spatially constant background (the first term). The background term is of the same order as V^{ph}. That is, an isolated quantum dot is not able to completely screen out an external potential. This behavior is based on particle conservation, for the charge on the dot can only be redistributed to some extent but cannot be increased or reduced via electrons flowing to or coming from the leads. Absorption and scattering of phonons are associated with the spatially varying component of the total potential which carries the factor $a_B/L \ll 1$. The screening of the SAW potential by the electrons in the quantum dot is thus an effect which reduces considerably the magnitude of the scattering and the absorption cross-sections.

In concluding this section let us consider the charge redistribution $\delta\rho(\boldsymbol{r})$. Substituting Eqs. (25) and (36) into Eq. (11) yields

$$\begin{aligned} \delta\rho(\boldsymbol{r}) &= -2\nu\delta(z-d) \sum_{m,n\geq 1} \psi_m(\boldsymbol{r}) \beta_{mn} V_n \\ &= -2\nu\delta(z-d) \frac{\pi a_B}{L} \sum_{m,n\geq 1} \psi_m(\boldsymbol{r}) (\tilde{G}^{-1})_{mn} V_n^{ph} + \mathcal{O}(a_B^2/L^2). \end{aligned} \tag{37}$$

That is, even in the strong screening case, where a_B is very small compared to other length scales, $\delta\rho(\boldsymbol{r})$ is determined by the distribution of the external potential within the whole dot. Indeed, the V_n^{ph} couple via non-diagonal elements of $\tilde{G}^{-1}$ to other modes m. In this sense, screening in an isolated dot is strongly non-local.

V. SCATTERING AND ABSORPTION CROSS-SECTIONS

In this section we study the absorption and the scattering cross-sections, Eqs. (1) and (2), in the limiting cases $qL \gg 1$ and $qL \ll 1$. We focus on the dependences of the cross-sections on q, D, and the area A of the dot, and on the qualitative influence of the

weak localization corrections. The substantiation of these analytical results by numerical calculations, addressing also the angular dependence of the cross-sections, their sensitivity to the shape of the dot, etc., will be deferred until Sec. VII.

A. The case $qL \gg 1$

This regime resembles the case of an infinitely extended system. One may therefore use the usual $\boldsymbol{q}$-space representation for the density-density correlator, the dielectric function, etc. This leads to the simple relation $V(\boldsymbol{r}) = V^{ph}_{\boldsymbol{q}}(\boldsymbol{r})/\epsilon(\omega, \boldsymbol{q})$ between the total potential and the SAW field. The dielectric function

$$\epsilon(\omega, \boldsymbol{q}) = 1 + \frac{2\pi e^2}{\epsilon_0 q}\left[1 + \frac{1-\epsilon_1/\epsilon_0}{1+\epsilon_1/\epsilon_0} e^{-qd}\right] 2\nu\beta(\omega, \boldsymbol{q}) \approx 1 + 2\frac{\beta(\omega, \boldsymbol{q})}{a_B q} \tag{38}$$

is derived form Eq. (16). Here,

$$\beta(\omega, \boldsymbol{q}) = \frac{(D+\delta D)q^2}{-i\omega + (D+\delta D)q^2} \tag{39}$$

is (except for the factor $-\nu$) the Fourier representation of the density-density correlator, Eq. (5), which replaces the expression β_{mn} [Eq. (25)] valid in the diffusion mode representation. To obtain Eq. (39), the weak localization correction $\delta D(\boldsymbol{r})$ to the diffusion coefficient [Eq. (23)] has been replaced by some average value $\delta D = \text{const}$, and, consequently, is not $\boldsymbol{r}$-dependent. Using $qd \ll 1$ and $\epsilon_1 = 1 \ll \epsilon_\circ$, the dielectric function simplifies to the result given on the right-hand-side of Eq. (38). The latter condition corresponds to vacuum above the surface of the semiconductor. The effective dielectric constant in the vicinity of the surface (distance smaller than $1/q$) is then given by $(\epsilon_\circ + \epsilon_1)/2 \approx \epsilon_\circ/2$.

Substituting the bare SAW potential [Eq. (8)] and the dielectric function $\epsilon(\omega, \boldsymbol{q})$ [Eq. (38)] in Eq. (7) for the quantity $\Pi_\omega(\boldsymbol{q}, \boldsymbol{q}')$, we obtain for the absorption cross-section [Eq. (1)]

$$\eta_{abs}(\boldsymbol{q})/A = \frac{4\nu}{s\hbar}|\gamma_{\boldsymbol{q}}|^2 \frac{\Im[\beta(\omega, \boldsymbol{q})]}{|\epsilon(\omega, \boldsymbol{q})|^2} \equiv \Gamma_{\boldsymbol{q}}. \tag{40}$$

The attenuation coefficient $\Gamma_{\boldsymbol{q}}$ is the relevant quantity for an extended system as it describes the decrease of the intensity of a SAW traveling a distance x along the surface as $\exp(-\Gamma_{\boldsymbol{q}} x)$. Note that $\eta_{abs}(\boldsymbol{q})$ does not possess the meaning of the total energy absorbed from the SAW once $\Gamma_{\boldsymbol{q}} L$ becomes larger than unity. Neglecting weak localization corrections, the attenuation coefficient given in Eq. (40) coincides with the result following from the well-known treatment of sound absorption due to the piezoelectric interaction [see, e.g., Refs.[12] and[19]]. In the case of strong screening, Eq. (40) can be written in the form

$$\Gamma_{\boldsymbol{q}} = \frac{\nu}{s\hbar}|\gamma_{\boldsymbol{q}}|^2 (a_B)^2 \frac{\omega}{D}\left(1 - \frac{\Re[\delta D]}{D}\right) = \frac{1}{2} K_{\rm eff}^2 q \frac{\sigma_m}{\sigma}\left(1 - \frac{\Re[\delta\sigma]}{\sigma}\right), \tag{41}$$

where the right-hand-side uses the "standard" notation, i.e. $\Gamma_{\boldsymbol{q}}$ is given in terms of the 2D conductivity σ, the conductivity $\sigma_m \equiv \epsilon_0 s/4\pi$, and the effective electromechanical coupling coefficient $K_{\rm eff}^2 = |\gamma_{\boldsymbol{q}}|^2 \epsilon_0 / 2\pi s e^2 \hbar$. Equation (41) does not only reproduce the well-known classical result for the absorption coefficient but gives also its dependence on the weak localization effects expressed in terms of δD or the weak localization correction $\delta\sigma$ of the conductivity. Since $\Re[\delta D] \sim \Re[\delta\sigma] < 0$, they enhance the absorption. The primary reason for this enhancement is the reduced screening caused by the slowing down of the diffusion processes. The enhancement factor $1 - \Re[\delta D]/D$ has been found in previous work[1,3–5] on the absorption of bulk sound in a 3D electron system or of (hypothetical) 2D phonons by a 2DEG, independent of whether the piezoelectric or the deformation potential electron-phonon interaction has been studied. A different result has been obtained in Ref.[2]. The reason for this, as discussed in Ref.[4], is the insufficient number of diagrams incorporated in that calculation.

Equation (2) for the scattering cross-section can be treated similarly. In the limit $qL \gg 1$, η_{sc} has a dominating forward-scattering component

$$\eta_{sc}(\boldsymbol{q}', \boldsymbol{q}) \sim \delta(\boldsymbol{q}' - \boldsymbol{q}). \tag{42}$$

This property results from the momentum conservation in a translational invariant system.

B. The case $qL \ll 1$

Here, we exploit the diffusion mode representation introduced in the previous two sections. Substituting the density-density correlator, Eq. (25), and the total potential in the strong screening limit, Eq. (36), into Eq. (7) yields

$$\Pi_\omega(\boldsymbol{q},\boldsymbol{q}') = -\nu\frac{(\pi a_B)^2}{A}\sum_{m,n,k,l\geq 1}(\beta^{-1})^*_{mn}(\tilde{G}^{-1})_{nk}(V^{ph}_k)^*(\tilde{G}^{-1})_{ml}V^{ph}_l. \tag{43}$$

Expanding the bare SAW potential [Eq. (8)] in a series with respect to $|\boldsymbol{qr}| \ll 1$, we find

$$\sum_{l\geq 1}(\tilde{G}^{-1})_{ml}V^{ph}_l = \frac{1}{\mathcal{L}}\gamma_{\boldsymbol{q}}iqAa_m(\hat{\boldsymbol{q}}), \tag{44}$$

where

$$a_m(\hat{\boldsymbol{q}}) \equiv \sum_{n\geq 1}(\tilde{G}^{-1})_{mn}\int\frac{d^2\boldsymbol{r}}{A}\,\hat{\boldsymbol{q}}\boldsymbol{r}\psi_n(\boldsymbol{r}). \tag{45}$$

The dimensionless integral in this equation is of order unity for small n's, and it decreases as n increases. $a_m(\hat{\boldsymbol{q}})$ is expected to have the same properties. Introducing result (44) in Eq. (43), we obtain

$$\Pi_\omega(\boldsymbol{q},\boldsymbol{q}') = -\nu(\pi a_B\gamma_{\boldsymbol{q}}q)^2A\mathcal{L}^{-2}\sum_{m,n\geq 1}(\beta^{-1})^*_{mn}a_m(\hat{\boldsymbol{q}})a_n(\hat{\boldsymbol{q}'}). \tag{46}$$

Up to first order in the weak localization corrections, the inverse of β_{mn}, Eq. (26), is given by

$$(\beta^{-1})_{mn} = \beta_m^{-1}\delta_{m,n} - \frac{\delta\beta_{mn}}{\beta_m\beta_n} \tag{47}$$

where $\delta\beta_{mn}$ is defined in Eq. (28).

We are now in the position to use Eq. (46) in the evaluation of the absorption and the scattering cross-sections. Substituting Eq. (46) into Eq. (1) yields

$$\begin{aligned}\eta_{abs}(\boldsymbol{q}) = {}& \frac{4\nu}{s\hbar}|\gamma_{\boldsymbol{q}}|^2(\pi a_B)^2q^2A^2\frac{\omega}{D} \\ & \times\sum_{m,n\geq 1}\frac{1}{A\lambda_m}\left(\delta_{m,n} - \frac{1}{\lambda_n}\int d^2\boldsymbol{r}\,\nabla\psi_m(\boldsymbol{r})\nabla\psi_n(\boldsymbol{r})\frac{\Re[\delta D(\boldsymbol{r})]}{D}\right)a_m(\hat{\boldsymbol{q}})a_n(\hat{\boldsymbol{q}}).\end{aligned} \tag{48}$$

Note that $A\lambda_m$ is a dimensionless quantity independent of A, cf. Eq. (20). A significant simplification of this equation is achieved when $\delta D(\boldsymbol{r})$ does not vary in space. This is not always the case, of course. We believe, however, that, qualitatively, the influence of the weak localization effects is described by an average quantity $\delta D = \text{const}$, which will be defined in Sec. VI. Replacing $\delta D(\boldsymbol{r})$ by δD and using the diffusion mode equation (20), Eq. (48) reduces to

$$\eta_{abs}(\boldsymbol{q}) = \frac{4\nu}{\hbar}|\gamma_{\boldsymbol{q}}|^2(\pi a_B)^2 A^2 \frac{q^3}{D}\left(1 - \frac{\Re[\delta D]}{D}\right)\left\{\sum_{m\geq 1}\frac{a_m^2(\hat{\boldsymbol{q}})}{A\lambda_m}\right\}. \tag{49}$$

The dependence on the shape of the dot and the direction of the SAW is comprised in the quantity in braces. The dependences on all other parameters is completely described by its prefactor. As in the case of an infinite system, Eq. (41), the weak localization corrections enhance the absorption. This can be again understood as a result of the reduced screening of the SAW potential. Comparing Eqs. (41) and (49) we see that η_{abs} is smaller by a factor (q^2A) in the case $qL \ll 1$. That is, a small system absorbs per unit area much less than an extended one. This can be attributed to the fact that the electrons in an extended system can move over the whole period $1/q$ of the piezoelectric field, while a small system restricts this motion by its size.

We shall now evaluate the scattering cross-section η_{sc}. Substituting Eq. (46) into Eq. (2) yields

$$\begin{aligned}\eta_{sc}(\boldsymbol{q'},\boldsymbol{q}) = {} & \frac{q\nu^2}{\pi s^2\hbar^2}(\pi a_B q)^4 A^2 \\ & \times \sum_{m,n,k,l\geq 1}(\beta^{-1})^*_{mn}(\beta^{-1})_{kl}a_m(\hat{\boldsymbol{q}}')a_n(\hat{\boldsymbol{q}})a_k(\hat{\boldsymbol{q}}')a_l(\hat{\boldsymbol{q}}).\end{aligned} \tag{50}$$

Here, we should replace the matrix elements of β^{-1} by the explicit expressions given in Eq. (47) and consider the classical and weak localization contributions separately. As far as the latter are concerned, we have to calculate the sum over four a-terms with the $\beta^{-1}\beta^{-1}$-part replaced by

$$-2\Re\left[\frac{1}{\beta_m^*}\frac{\delta\beta_{kl}}{\beta_k\beta_l}\right].$$

This can be rewritten as

$$-2\frac{\omega}{D^2\lambda_k\lambda_l}\int d^2\boldsymbol{r}\,\nabla\psi_k(\boldsymbol{r})\nabla\psi_l(\boldsymbol{r})\{\Im[\delta D(\boldsymbol{r})]+\frac{\omega}{D\lambda_m}\Re[\delta D(\boldsymbol{r})]\}, \tag{51}$$

showing that the relevant quantity is either $\Re[\delta D(\boldsymbol{r})]$ or $\Im[\delta D(\boldsymbol{r})]$ depending on whether the diffusion time through the dot, A/D, is large or small compared to the period of the SAW potential.

The replacement of $\delta D(\boldsymbol{r})$ by δD =const leads to a considerable simplification of expression (51). Using this approximation to evaluate Eq. (50), we obtain explicit estimates in the limits of a small and a big dot:

$$\begin{aligned}\eta_{sc}(\boldsymbol{q'},\boldsymbol{q}) \approx{}& \frac{\nu^2}{\pi s^2\hbar^2}|\gamma_{\boldsymbol{q}}|^2|\gamma_{\boldsymbol{q}'}|^2(\pi a_B)^4 q^5 A^2 \\ &\times\sum_{m\geq 1}a_m(\hat{\boldsymbol{q}}')a_m(\hat{\boldsymbol{q}})\sum_{n\geq 1}a_n(\hat{\boldsymbol{q}}')a_n(\hat{\boldsymbol{q}})\{1-2\frac{\omega}{D\lambda_n}\frac{\Im[\delta D]}{D}\} \quad \omega A/D\ll 1 \\ &\times\left(\sum_{m\geq 1}\frac{a_m(\hat{\boldsymbol{q}}')a_m(\hat{\boldsymbol{q}})}{A\lambda_m}\right)^2\left(\frac{\omega A}{D}\right)^2\{1-2\frac{\Re[\delta D]}{D}\} \qquad \omega A/D\gg 1\end{aligned} \tag{52}$$

The classical contribution and the prefactor of the weak localization corrections to the scattering cross-section depend strongly on the parameter $A\omega/D$. For a big dot, $A\omega/D>1$, the scattering of SAW's rises faster than A^2 with increasing area A of the dot because the diffusion processes are too slow to screen long wavelength density variations as effectively as short wavelength ones. Indeed, the enhancement factor $\omega A/D$ results from the classical part of $(\beta^{-1})_{mn}$, $\beta_m^{-1}=1-i\omega/D\lambda_m$ [Eq. (28)], which enters Eq. (50) via the inverse of the dielectric matrix. In the small dot case, $\beta_m^{-1}\simeq 1$ for all m starting from unity, and, hence, there is no enhancement factor in the second line of Eq. (52). While the quantum corrections contribute to η_{sc} according to their relative magnitude for big dots, they acquire a small prefactor once $\omega A/D$ becomes smaller than unity. Moreover, since their imaginary part is the relevant quantity in that case, they are small for $\omega<\tau_\phi^{-1}$, cf. Eq. (64) below. This is contrary to the dependence of weak localization corrections on frequency and phase coherence time as far as the real part of the conductivity is concerned.

VI. WEAK LOCALIZATION CORRECTIONS

The absorption and the scattering cross-sections depend on weak localization corrections via $\delta D(\boldsymbol{r})$ which in turn is directly related to the cooperon $\mathcal{C}_\omega(\boldsymbol{r},\boldsymbol{r})$; see Eq. (23). In the first part of this section, we evaluate the cooperon equation (24). Special attention is devoted to the magnetic field dependence. In the second part, we discuss the approximation of $\delta D(\boldsymbol{r})$ by a spatially independent quantity δD.

A. Magnetic field dependence

In comparison with the diffusion propagator, Eq. (19), the cooperon, Eq. (24), depends on the two additional length scales $l_\phi = \sqrt{D\tau_\phi}$ and $l_B = \sqrt{c\hbar/2eB}$. Due to the sensitivity of quantum corrections to weak magnetic fields, it is sufficient to account perturbatively for the B-dependent terms in Eq. (24). To this end, we expand the cooperon in a power series with respect to $\boldsymbol{A}(\boldsymbol{r})$:

$$\mathcal{C}_\omega(\boldsymbol{r},\boldsymbol{r}') = \mathcal{C}_\omega^{(0)}(\boldsymbol{r},\boldsymbol{r}') + \mathcal{C}_\omega^{(1)}(\boldsymbol{r},\boldsymbol{r}') + \mathcal{C}_\omega^{(2)}(\boldsymbol{r},\boldsymbol{r}') + \ldots, \tag{53}$$

where $\mathcal{C}_\omega^{(m)} \sim \boldsymbol{A}^m$. This expansion can be terminated with a negligible error at the first nonvanishing correction to $\mathcal{C}_\omega^{(0)}(\boldsymbol{r},\boldsymbol{r})$ if $L/l_B \ll 1$ and $|-i\omega+\tau_\phi^{-1}| \gg DL^2/l_B^4$. Using experimental values [which are summarized in Sec. VII], we have $\omega \lesssim \tau_\phi^{-1}$, i.e. the second inequality can be written as $Ll_\phi/l_B^2 \ll 1$. Since $l_\phi \lesssim L$ in the cases of practical interest, the first condition $L/l_B \ll 1$ determines the range of applicability of the perturbative treatment. Substituting Eq. (53) in Eq. (24) yields

$$\begin{aligned}
&[-i\omega+\tau_\phi^{-1}-D\nabla^2]\mathcal{C}_\omega^{(0)}(\boldsymbol{r},\boldsymbol{r'}) = \delta(\boldsymbol{r}-\boldsymbol{r'}),\\
&[-i\omega+\tau_\phi^{-1}-D\nabla^2]\mathcal{C}_\omega^{(1)}(\boldsymbol{r},\boldsymbol{r'}) = -2iD(2e/c\hbar)\boldsymbol{A}(\boldsymbol{r})\nabla\mathcal{C}_\omega^{(0)}(\boldsymbol{r},\boldsymbol{r'}),\\
&[-i\omega+\tau_\phi^{-1}-D\nabla^2]\mathcal{C}_\omega^{(2)}(\boldsymbol{r},\boldsymbol{r'}) = -2iD(2e/c\hbar)\boldsymbol{A}(\boldsymbol{r})\nabla\mathcal{C}_\omega^{(1)}(\boldsymbol{r},\boldsymbol{r'}) - D((2e/c\hbar)\boldsymbol{A}(\boldsymbol{r}))^2\mathcal{C}_\omega^{(0)}(\boldsymbol{r},\boldsymbol{r'}),
\end{aligned} \tag{54}$$

where we have used the gauge $\nabla\boldsymbol{A}(\boldsymbol{r}) = 0$. The boundary conditions are given by

$$\nabla_n \mathcal{C}_\omega^{(0)}|_b = 0, \qquad \nabla_n \mathcal{C}_\omega^{(m+1)}|_b = i(2e/c\hbar)\boldsymbol{A}_n \mathcal{C}_\omega^{(m)}|_b, \text{ for } m = 0, 1, \ldots . \tag{55}$$

The equation for $\mathcal{C}_\omega^{(0)}$ can be solved using the diffusion modes defined in Eq. (20)

$$\mathcal{C}_\omega^{(0)}(\boldsymbol{r}, \boldsymbol{r}') = \sum_{m=0}^{\lambda_m \lesssim l^{-2}} \frac{\psi_m(\boldsymbol{r})\psi_m(\boldsymbol{r}')}{-i\omega + D\lambda_m + \tau_\phi^{-1}}. \tag{56}$$

The cut-off on the summation is because the diffusion approximation is valid on scales larger than the mean free path. The relevant frequency scale is given by $|-i\omega + \tau_\phi^{-1}|$.

Since $\mathcal{C}_\omega^{(0)}$, Eq. (56), is the Green's function for the differential operator of all three equations (54), it enables us to write down formal solutions for $\mathcal{C}_\omega^{(1)}$ and $\mathcal{C}_\omega^{(2)}$ as well. The result for $\mathcal{C}_\omega^{(1)}$ reads

$$\begin{aligned}\mathcal{C}_\omega^{(1)}(\boldsymbol{r}, \boldsymbol{r'}) = D \oint d\boldsymbol{S}_1 \, [i(2e/c\hbar)\boldsymbol{A}_n(\boldsymbol{r}_1)\mathcal{C}_\omega^{(0)}(\boldsymbol{r}_1, \boldsymbol{r'})]\mathcal{C}_\omega^{(0)}(\boldsymbol{r}_1, \boldsymbol{r}) \\ + \int d^2\boldsymbol{r}_1 \, [-2iD(2e/c\hbar)\boldsymbol{A}(\boldsymbol{r}_1))\nabla_1 \mathcal{C}_\omega^{(0)}(\boldsymbol{r}_1, \boldsymbol{r'})]\mathcal{C}_\omega^{(0)}(\boldsymbol{r}_1, \boldsymbol{r}).\end{aligned} \tag{57}$$

The first term accounts for the source term in the differential equation, whereas the second one represents an integral over the boundary of the dot and includes the inhomogeneity of the boundary condition (55). Equation (57) can be rewritten in the symmetric form

$$\mathcal{C}_\omega^{(1)}(\boldsymbol{r}, \boldsymbol{r'}) = \int d^2\boldsymbol{r}_1 \, i(2e/c\hbar)\boldsymbol{A}(\boldsymbol{r}_1)\nabla_1 [\mathcal{C}_\omega^{(0)}(\overset{\downarrow}{\boldsymbol{r}}_1, \boldsymbol{r})\mathcal{C}_\omega^{(0)}(\boldsymbol{r}_1, \boldsymbol{r'}) - \mathcal{C}_\omega^{(0)}(\overset{\downarrow}{\boldsymbol{r}}_1, \boldsymbol{r'})\mathcal{C}_\omega^{(0)}(\boldsymbol{r}_1, \boldsymbol{r})], \tag{58}$$

where the arrow indicates the argument upon which the derivative acts. The last equation shows that $\mathcal{C}_\omega^{(1)}(\boldsymbol{r}, \boldsymbol{r}) = 0$, i.e. the quantum corrections to the diffusion coefficient (23) do not depend linearly on the magnetic field. The expression for $\mathcal{C}_\omega^{(2)}$ has the same structure as Eq. (57), one has just to substitute the corresponding source terms given in Eqs. (54). That is,

$$\begin{aligned}\mathcal{C}_\omega^{(2)}(\boldsymbol{r}, \boldsymbol{r'}) = D \oint d\boldsymbol{S}_1 \, [i(2e/c\hbar)\boldsymbol{A}_n(\boldsymbol{r}_1)\mathcal{C}_\omega^{(1)}(\boldsymbol{r}_1, \boldsymbol{r'})]\mathcal{C}_\omega^{(0)}(\boldsymbol{r}_1, \boldsymbol{r}) \\ + \int d^2\boldsymbol{r}_1 \, [-2iD(2e/c\hbar)\boldsymbol{A}(\boldsymbol{r}_1))\nabla_1 \mathcal{C}_\omega^{(1)}(\boldsymbol{r}_1, \boldsymbol{r'}) - D((2e/c\hbar)\boldsymbol{A}(\boldsymbol{r}_1))^2 \mathcal{C}_\omega^{(0)}(\boldsymbol{r}_1, \boldsymbol{r'})]\mathcal{C}_\omega^{(0)}(\boldsymbol{r}_1, \boldsymbol{r}).\end{aligned} \tag{59}$$

This equation and Eq. (56) determine the weak localization correction to the diffusion coefficient in the form $\delta D(\boldsymbol{r}) = -(D/\pi\hbar\nu)(\mathcal{C}_\omega^{(0)}(\boldsymbol{r}, \boldsymbol{r}) + \mathcal{C}_\omega^{(2)}(\boldsymbol{r}, \boldsymbol{r}))$. Since $\mathcal{C}_\omega^{(2)} \sim B^2$, the physical quantities calculated in the previous section are invariant with respect to a reversal of the direction of the magnetic field.

B. The average quantity δD

The spatially constant quantity δD which was used in Sec. V is introduced by

$$\delta D(\boldsymbol{r}) \longrightarrow \delta D \equiv -\frac{D}{\pi\hbar\nu A}\int d^2\boldsymbol{r}\,\mathcal{C}_\omega(\boldsymbol{r},\boldsymbol{r}). \tag{60}$$

This approximation captures the essential features of the problem and becomes exact in two limiting cases. For small frequencies and large phase coherence times, $|-i\omega+\tau_\phi^{-1}| \ll D/A$, the cooperon is determined by the zeroth diffusion mode ψ_0, and hence $\mathcal{C}_\omega(\boldsymbol{r},\boldsymbol{r})$ ≈const. In the opposite case, the bulk-like diffusion process guarantees that at least $\mathcal{C}^{(0)}_\omega(\boldsymbol{r},\boldsymbol{r})$ is spatially uniform except near the boundaries. In the intermediate regime, $|-i\omega+\tau_\phi^{-1}| \simeq D/A$, we expect a smooth cross-over between these two limiting cases.

In the limiting cases one is able to obtain explicit results for the averaged weak localization correction δD in the following way. Depending on whether $A|-i\omega+\tau_\phi^{-1}|/D$ is smaller or larger than unity, it is convenient to replace the zero-field cooperon $\mathcal{C}^{(0)}_\omega$ in the solution for $\mathcal{C}^{(2)}_\omega$, Eq. (59), by its diffusion mode representation (56) or its Fourier representation for an infinite 2D system

$$\mathcal{C}^{(0)}_\omega(\boldsymbol{r},\boldsymbol{r}') = \int \frac{d^2\boldsymbol{q}}{(2\pi)^2}\,\frac{e^{i\boldsymbol{q}(\boldsymbol{r}-\boldsymbol{r}')}}{-i\omega+Dq^2+\tau_\phi^{-1}}, \tag{61}$$

respectively. In the former case, we are able to separate the large contributions due to the zero-mode from the corrections resulting from all other modes. In the latter, the particle diffuses on scales small compared to the size of the system; hence, the boundary conditions imposed on a finite dot can be disregarded.

1. Small dot case

Substituting Eq. (56) in $\mathcal{C}^{(2)}_\omega$, Eq. (59), yields

$$\int d^2\boldsymbol{r}\,\mathcal{C}_\omega(\boldsymbol{r},\boldsymbol{r}) = \sum_{m=0}^{\lambda_m\lesssim l^{-2}}\Bigg[-i\omega+D\lambda_m+\tau_\phi^{-1}+ \\ +D\int d^2\boldsymbol{r}\,\psi_m^2(\boldsymbol{r})(2e\boldsymbol{A}(\boldsymbol{r}))^2+D^2\sum_{n=0}^{\lambda_n\lesssim l^{-2}}\frac{(F_{nm}-F_{mn})^2}{-i\omega+D\lambda_n+\tau_\phi^{-1}}\Bigg]^{-1}, \tag{62}$$

where

$$F_{mn} = \int d^2\boldsymbol{r}\, \psi_m(\boldsymbol{r}) i2e\boldsymbol{A}(\boldsymbol{r})\nabla\psi_n(\boldsymbol{r}). \tag{63}$$

For $A|-i\omega+\tau_\phi^{-1}|/D<1$, we restrict the sum to the $m=0$ term and obtain

$$\delta D = -\frac{D}{\pi\hbar\nu A}\,\frac{1}{-i\omega+\tau_\phi^{-1}+c_1 DA/l_B^4}, \tag{64}$$

where c_1 is a real positive constant of order unity. The lowest eigenmode ψ_0 leads to an increase of the weak localization corrections as the area A of the dot decreases. This behavior results from the fact that the boundaries of an isolated system cause no phase-breaking. In the case where the dot is connected to leads, the summation over modes starts at $m=1$ and yields[23] $\delta D = -(\pi\hbar\nu)^{-1}\ln(A/l^2)$ for $B=0$. That is, the correction term decreases as the dot shrinks. The reduction of the size of the system is then associated with contacts approaching each other, which leads in turn to a decrease of the phase coherence. The scales of the critical magnetic field at which the phase coherence is significantly reduced are different for isolated and open systems as well. The critical magnetic field can be deduced from Eq. (62) by equating the two magnetic field dependent terms [which are of the same order] to the first one. For an isolated dot, the first term is of order $|-i\omega+\tau_\phi^{-1}|$, Eq. (64), whereas it is given by D/A for a dot coupled to leads. This results in the estimates

$$(l_B^4)^{iso} \simeq A\min\{D/\omega, l_\phi^2\} \qquad \text{and} \qquad (l_B^4)^{lead} \simeq A^2. \tag{65}$$

The critical magnetic field for an isolated small dot is thus much larger than for a dot with leads.

2. Big dot case

For $A|-i\omega+\tau_\phi^{-1}|/D>1$, we substitute Eq. (61) in $\mathcal{C}_\omega^{(2)}$, Eq. (59), and obtain

$$\delta D = \frac{c_2}{\pi\hbar\nu}\,\ln\left\{\tau[-i\omega+\tau_\phi^{-1}+c_3 DA/l_B^4]\right\}, \tag{66}$$

where c_2 and c_3 are real positive constants of order unity. In this case, the zeroth mode plays no role; Eq. (66) is valid independently of the boundary conditions imposed.

The results (64) and (66) for δD can be substituted in Eqs. (41), (49), and (52) for the absorption coefficient and the cross-sections, respectively, in order to account explicitly for the weak localization corrections. Note, however, that the characterization as "big" or "small" dot does not necessarily apply simultaneously to both the diffusion propagator [Eq. (19)] and the cooperon [Eq. (56)]. In particular, for $\omega\tau_\phi \ll 1$, there exists the situation where the diffusion propagator [responsible for the classical contributions] is determined by the zeroth mode since $A\omega/D \ll 1$, whereas the cooperon [determining δD] behaves bulk-like since $A\tau_\phi^{-1}/D \gg 1$.

VII. NUMERICAL CALCULATIONS

To compute numerically the scattering and the absorption cross-sections, we have used an accurate inversion of the dielectric function $\epsilon(\boldsymbol{r}, \boldsymbol{r'})$, which in turn yields the total potential V, see Eqs. (30) and (33). This exact procedure covers small and large values of the parameter qL. In this sense, the numerical results bridge the gap left by the analytical study of limiting cases in Sec. V, and provide information about the angular dependence of the cross-sections. The scaling of the numerically calculated cross-sections with respect to A, q, D etc. can be used to confirm the predictions derived analytically, cf. Eqs. (41)–(52). In Figs. 3–5 discussed below, results for different wave vectors q are shown; all other parameters are kept fixed. This means that the two dimensionless quantities qL and $A\omega/D$ vary. Since the latter, even for the largest wave vectors used is smaller than unity, it is essentially the effects of the variation of qL which we focus on. In this small dot case, the weak localization corrections are essentially described by the quantity $1 - \Re[\delta D]/D$, cf. Eqs. (49) and (52). The dependence of this quantity on magnetic field, frequency and temperature is discussed in connection with Fig. 6.

The dot has the shape of a square (lengths $L_x = L_y$) or a rectangle ($L_x > L_y$). In the first

case emphasis is put on the angular dependence associated with the value of the parameter qL. The eigenfunctions are given by $\psi_{m_x,m_y}(x,y) \sim \cos(m_x \pi x/L_x)\cos(m_y \pi y/L_y)$, where m_x and m_y are positive integers starting from zero. The number of diffusion modes for each direction is restricted to, e.g., $m_x^{max} = m_y^{max} = 12$ for the square and to $m_x^{max} = 20$, $m_y^{max} = 8$ for the rectangle discussed in Fig. 4. Hence, the total number of different modes, which coincides with the dimension of the matrices ϵ_{mn}, G_{mn}, etc., is $12^2 = 144$ or $20 \times 8 = 160$, respectively.

The numerical calculations are based on values for the physical quantities which apply to GaAs/Al_xGa_{1-x}As heterostructures: $\nu = 1.55 \times 10^{10}$ meV^{-1}cm^{-2}, $s = 2.7 \times 10^5$ cms^{-1}, $D = 140$ cm^{2}s^{-1} [$l = 0.1$ μm], $\tau = 0.4$ ps, $\tau_\phi = 0.03$ ns, $d = 0.1$ μm, $a_B = 10.6$ nm, $\epsilon_\circ = 12.8$, $\epsilon_1 = 1$, and, e.g., $L_x = L_y = 0.66$ μm for the square dot. The phase coherence time (corresponding to $T = 0.1$ K and $l_\phi = 0.63$ μm) and the diffusion coefficient for a low mobility electron gas are taken from Ref.[24]. The selection of a small diffusion coefficient is dictated by the condition that the size of the dot is larger than the mean free path, but small enough to allow for $qL < 1$ and $qL > 1$ in the range of reasonable sound frequencies. For these frequencies and the quantities given above, ω and τ_ϕ^{-1} are smaller than D/A. Thus, the diffusion propagator [Eq. (19)] and the cooperon [Eq. (56)] are essentially determined by the zeroth mode. Since the very existence of the zeroth mode relies on the assumption of an isolated dot, it is this physical regime which puts most emphasis on the noninvasive character of the proposed SAW measurement. Posing the requirement $q < l^{-1}$ yields $q \approx 10^5$ cm^{-1} ($\omega \approx 2\pi \times 4.3$ GHz) as the upper limit for the applicability of the diffusion approximation. A lower limit $\omega > \Delta$ could arise from the finiteness of the mean level spacing $\Delta = (\nu A)^{-1}$ in the quantum dot. For $A \simeq 1$ μm^2, we have $\Delta \simeq 6$ μeV corresponding to $\omega \simeq 10^{10}$ s^{-1}. We argue, however, that inelastic level broadening smears out the discreteness of the one-particle levels, rendering the spacing Δ irrelevant. Indeed, using the phase coherence time introduced above, we find $\hbar/\tau_\phi \simeq 20$ μeV $> \Delta$. That is, a lower limit for the frequency is not required.

Figure 3 shows in a double-logarithmic plot the absorption and the scattering cross-

sections, Eqs. (1) and (2), as a function of the wave vector. Here and in Figs. 4 and 5 the term $\hat{q}_x\hat{q}_y$ of the electron-surface phonon vertex, Eq. (9), has been replaced by its maximum $\frac{1}{2}$; its angular dependence is not taken into account because it depends on the orientation of the dot with respect to the lattice axes. Quantum corrections for $B = 0$ are incorporated and $L_x = 1.7$ μm and $L_y = 1$ μm. The inset in Fig. 3 shows the correct aspect ratio of the dot, the direction of the incoming SAW (unlabeled arrow), and the direction of the outgoing SAW for a scattering angle of 30° (arrow 2). The corresponding absorption cross-section $\eta_{abs}(\boldsymbol{q})$ is given by curve 1. The part to the left of label 1 exhibits the behavior $\eta_{abs} \sim q^3$, confirming the power law predicted by Eq. (49) for the limit $qL \ll 1$. The remaining part of the curve corresponds to $\eta_{abs} \sim q$. This behavior is anticipated in the regime $qL \gg 1$; see Eq. (41). The oscillations of $\eta_{abs}(\boldsymbol{q})$ represent geometric resonances. Maxima appear around $qL_x = 2\pi m$, $m = 1, 2, \ldots$, whereas minima occur for $qL_x = \pi(2m + 1)$. The curve labeled 2 (corresponding to the direction 2) represents results for the scattering cross-section. It follows the power law $\eta_{sc} \sim q^5$, Eq. (52), in the limit $qL \ll 1$. For $qL \gg 1$, the scattering cross-section behaves in a sample and angle specific way. In this case, the magnitude of $\eta_{sc}(\boldsymbol{q}' \neq \boldsymbol{q})$ is small compared to the forward scattering component which continues to grow as q^5, cf. relation (42) and Fig. 5. Taking the results for both η_{abs} and η_{sc} into account, one may conclude that the limiting equations for $qL \ll 1$ and $qL \gg 1$ given in Sec. V represent a good description up (or down) to $qL \approx 2\pi$.

Figure 4 shows results for the absorption cross-section, Eq. (1), of a rectangular (main plot) and a square dot (inset). The size of the dots is given by $L_x = 1.2$ μm and $L_y = 0.4$ μm and $L_x = L_y = 0.66$ μm, respectively. The abscissa of the figure agrees with the x-axis of the dot. Figure 4 represents a polar diagram for $\eta_{abs}(\boldsymbol{q})$, i.e. the distance of a data point from the origin corresponds to the magnitude of η_{abs} [given in μm], whereas the orientation of the wave vector $\boldsymbol{q}$ of the SAW agrees with the direction of the line joining the data point and the origin. The curves labeled 1, 2, and 3 correspond to the wave vectors $q_1 = 10^4$ cm^{-1}, $q_2 = 5 \times 10^4$ cm^{-1}, and $q_3 = 10^5$ cm^{-1}, respectively. The magnitude of the curves labeled 1 is increased by a factor of 20. The main plot in Fig. 4 for the rectangular dot shows a strong

anisotropy of the absorption cross-section for the two smaller wave vectors. For instance, $\eta_{abs}(q_1\hat{x})$ and $\eta_{abs}(q_1\hat{y})$ deviate by a factor of about 20 from each other. This pronounced anisotropy can be attributed to the fact that the relevant size of the dot (either L_x or L_y) enters Eq. (49) for η_{abs} as a high power in the limit $qL < 1$. In contrary, for the largest wave vector q_3, $\eta_{abs}(\boldsymbol{q})$ exhibits only a minor dependence on the angle of incidence, reflecting that only the total area is relevant in the regime $qL \gg 1$, cf. Eq. (40). That is, for an approximate isotropy of $\eta_{abs}(\boldsymbol{q})$ to appear, both qL_x and qL_y have to be sufficiently larger than unity. As can be seen from the inset of Fig. 4, the situation is somewhat different in the case of a square dot. Here, $\eta_{abs}(\boldsymbol{q})$ is completely independent of the direction of incidence for the smallest wave vector q_1. The absorption cross-section acquires a weak angular dependence with increasing wave vector which can be attributed to geometrical resonances occurring for $qL \geq 2\pi$.

All the curves presented in Fig. 4 include weak localization corrections to the density-density correlator, Eq. (28), for zero magnetic field. As discussed in Sec. V, the absorption is increased by these effects. This enhancement is expected to be given by a factor $1 - \Re[\delta D]/D$ independent of q for the "small-dot" case, cf. Eqs. (49) and (64). Indeed, all numerical calculations indicated that the curves with and without quantum corrections exhibit practically the same angular dependence, merely the magnitudes differ by a constant factor. Because of this, we do not incorporate in Fig. 4 curves which deviate from each other only with respect to the magnitude of the weak localization corrections. Instead, we discuss the enhancement factor $1 - \Re[\delta D]/D$ separately below.

Figure 5 presents results for the elastic scattering cross-section, Eq. (2), of a square dot. $\eta_{sc}(\boldsymbol{q'}, \boldsymbol{q})$ is given in μm. A polar representation is chosen with respect to the direction of the outgoing surface phonon $\hat{\boldsymbol{q'}}$. The direction of incidence, $\hat{\boldsymbol{q}}$, is fixed and is oriented perpendicularly to one of the edges of the square dot, see the inset. The labels 1, 2, and 3 of the curves indicate the wave vectors used, $q_3 = 2q_2 = 10q_1 = 10^5$ cm^{-1}. However, due to the significant dependence of η_{sc} on the magnitude of q, a normalization of the curves different from that of Fig. 4 is required: the data of curve 1 are multiplied by 10^3, while that of curve 3

are divided by 15 and those of curve 2 are not changed. Generally, the scattering cross-section of the square dot shows a weak dependence on the angle of incidence but varies considerably with the scattering angle θ, i.e. $\theta = \sphericalangle(\hat{\boldsymbol{q}}', \hat{\boldsymbol{q}})$. In particular, the angular dependence of η_{sc} in the regime $qL < 1$ [curve 1] is given by $\eta_{sc} \sim \cos^2\theta = (\hat{\boldsymbol{q}}\hat{\boldsymbol{q}'})^2$. This behavior could be anticipated from the equations given in Sec. V, taking into account not only the magnitude of the wave and spatial vectors but also their orientation. With increasing wave number q, the $\cos^2\theta$-law is gradually replaced by an enhancement of forward scattering and a suppression of back scattering. [This is known in the theory of electromagnetic fields as Mie effect, cf. Ref.[25], p. 654.] For $q = q_2$, only a small back-scattering component is left. For even larger q, e.g. $q = q_3$, this component is not resolved on the scale of Fig. 5. This confirms Eq. (42). In agreement with our qualitative analysis, quantum corrections are extremely small for the parameters introduced above. The curves in Fig. 5 correspond therefore essentially to the classical part of the scattering cross-section.

In the small dot case under consideration, the weak localization corrections to the absorption cross-section are significant, whereas the scattering cross-section remains practically unaffected. According to the analytically derived expressions (41) and (49) and the numerical calculations, these corrections to η_{abs} are well described by the enhancement factor $1 - \Re[\delta D]/D$. To illustrate the dependence of the weak localization corrections to η_{abs} on the perpendicular magnetic field B, the frequency and the temperature, we have evaluated $1 - \Re[\delta D]/D$ for the cooperon expression (62). For the small dot, $A|-i\omega + \tau_\phi^{-1}|/D \ll 1$, we expect δD to be determined by the lowest mode. According to Eq. (64),

$$-\delta D/D = \Delta\tau_\phi/\pi\hbar = 0.23, \tag{67}$$

where we have used $\omega < \tau_\phi^{-1}$ and $B = 0$. The right-hand side follows from the numerical values introduced above. In Fig. 6, $1 - \Re[\delta D]/D$ is shown as a function of the magnetic field. The dot is assumed to be of a square shape with $L_x = L_y = 0.66$ μm. All other parameters are as defined above. The deviations of the numerical results from the estimate (67) arise from the contributions of the higher modes. The assumption $l_B > L$, used to

derive the terms in the cooperon which depend on the magnetic field, is valid for $B < 1.4$ mT. The continuation of the curves to stronger magnetic fields can only serve as an indication for the further suppression of the weak localization corrections with increasing B. The three curves in Fig. 6 show how the quantity $1 - \Re[\delta D]/D$ decreases with increasing frequency. Assuming[24] $\tau_\phi \sim T^{-1}$, the increase of the temperature from $T = 0.1$ K to $T = 1$ K corresponds to a reduction of the phase coherence length from $l_\phi = 0.63$ μm [which is used in Fig. 6] to $l_\phi = 0.2$ μm. The latter value is significantly smaller than the size of the dot, $L = 0.66$ μm, leading to $1 - \Re[\delta D]/D \approx 1.07$ for $B = 0$. The relative differences between the three curves shown in Fig. 6 become much smaller as well.

VIII. CONCLUSIONS

We have calculated the absorption and the scattering cross-sections, $\eta_{abs}(\boldsymbol{q})$ and $\eta_{sc}(\boldsymbol{q}', \boldsymbol{q})$, respectively, of a surface acoustic wave [SAW] for an isolated quantum dot. The dependence of these quantities on weak localization corrections has been found. In addition, we have calculated the weak localization corrections to the attenuation coefficient $\Gamma_{\boldsymbol{q}}$ of an extended 2DEG [Eq. (41)]. Since these corrections can (at least) approximately be expressed in terms of δD, the spatial average of the corresponding change of the diffusion coefficient [Eq. (60)], they are given in a similar way as those to the conductivity. One can therefore use results derived in that case to establish easily the dependence of the cross-sections and $\Gamma_{\boldsymbol{q}}$ on spin-orbit scattering, scattering by magnetic impurities, etc.[21] We emphasize the weak localization corrections because they are expected to play a significant role in the experimental investigation of the effects discussed in this paper. Indeed, though the classical cross-sections depend strongly on A and ω, these parameters are fixed once the dot and interdigital transducers are defined on a sample. Measurements at different frequencies or at other sizes of the dot require the preparation of different samples. The proximity technique[13,12] may reduce the experimental effort, but it still provides only a set of discrete frequencies ω at which a certain sample can be studied. Conversely, it poses no serious

problems to vary continuously the temperature and the magnetic field which both affect only the weak localization corrections. Note also that the SAW technique allows precise measurements of the relative changes of the transmitted wave intensity, whereas the absolute attenuation is much less easily detectable. That is, the large but constant classical effects are generally more difficult to resolve than the quantum corrections which can be "tuned" by external parameters. For example, the measurement of the absorption cross-section (or $\Gamma_{\boldsymbol{q}}$) as a function of the temperature yields directly the dependence of the phase coherence time on the temperature. For typical experimental values, $\omega\tau_\phi < 1$, and, hence, the parameter A/l_ϕ^2 determines whether the dot has to be considered as a small or big one. Consequently, the temperature can also shift the dot from one regime to another.

Depending on the sensitivity of the methods used to measure SAW's, an experimental investigation might be carried out for an array of quantum dots rather than a single dot. Since the electron-phonon coupling is weak (even for the piezoelectric interaction), it is reasonable to assume that the response of a dot array to a SAW can be represented by a superposition of the effects associated with isolated dots. To underscore this point, let us give some numerical estimates for the SAW attenuation and the electron heating. To estimate whether the calculated cross-sections are within the experimental sensitivity, we convert the absorption cross-section to an attenuation coefficient by $\Gamma_{\boldsymbol{q}} \simeq \eta_{abs}/A$, cf. Eq. (40). This amounts to covering densely the area between the transducers with quantum dots. Using $\eta_{abs} \simeq 10^{-4}$ μm and $A \simeq 1$ μm^2 yields an attenuation of about 10 dB/cm. The relative change of the attenuation due to weak localization effects is then about 1 dB/cm. This value is about 10 times larger than the highest resolution achieved, suggesting that the signal of a much less dense arrangement of dots can be measured.

To estimate the effect of electron heating, one has to compare the temperature of the dot with $\Delta T \equiv I\eta_{abs}\tau_\epsilon/k_B$, where I is the flux intensity of the incoming surface wave, τ_ϵ is the energy relaxation time and k_B is the Boltzmann constant. Using $w \approx 2$ mm for the length and the width of a macroscopic SAW delay line and $P \approx 1$ μW for the total SAW intensity, we determine $I = P/w$ [the experimental values are taken from Ref.[13]]. The

energy relaxation time τ_ϵ can roughly be identified with the phase coherence time τ_ϕ. [We note that this is a good estimate in the case where both τ_ϵ and τ_ϕ result from electron-electron scattering; see Ref.[21].] Using the values $\tau_\phi = 30$ ps and $\eta_{abs} \simeq 10^{-4}$ μm, we obtain $\Delta T \simeq 0.1$ K which represents a significant change in the temperature range of interest.

ACKNOWLEDGMENTS

Financial support by the German-Israeli Foundation, the Fund for Basic Research administered by the Israel Academy of Sciences and Humanities, and the Deutsche Forschungsgemeinschaft (A. K.) is gratefully acknowledged. We thank Y. Galperin, A. Kamenev, D. Khmelnitzkii, D. Klakow, C. Rocke, M. Rotter, A. Tilke, and A. Wixforth for valuable discussions.

REFERENCES

[1] A. Houghton and H. Won, J. Phys. C **18**, 2507 (1985).

[2] G. Kotliar and T. V. Ramakrishnan, Phys. Rev. B **31**, 8188 (1985).

[3] V. V. Afonin, Y. M. Galperin, and R. N. Ignat'ev, Fiz. Tverd. Tela (Leningrad) **28**, 1063 (1986) [Sov. Phys. Solid State **28**, 594 (1986)].

[4] T. R. Kirkpatrick and D. Belitz, Phys. Rev. B **34**, 2168 (1986).

[5] M. Y. Reizer, Phys. Rev. B **40**, 7461 (1989).

[6] R. A. Serota, Phys. Rev. B **38**, 12640 (1988).

[7] S. Hershfield and M. Y. Reizer, Phys. Rev. B **43**, 9475 (1991).

[8] G. W. Farnell, in *Acoustic Surface Waves*, edited by A. A. Oliner (Springer, Berlin, 1978).

[9] A. Mayer, Phys. Rep. **256**, 237 (1995).

[10] V. W. Rampton, K. McEnaney, A. G. Kozorezov, P. J. A. Carter, C. D. W. Wilkinson, M. Henin, and O. H. Hughe, Semicond. Sci. Technol. **7**, 641 (1992).

[11] A. Wixforth, J. P. Kotthaus, and G. Weimann, Phys. Rev. Lett. **56**, 2104 (1986).

[12] A. Wixforth, J. Schriba, M. Wassermeier, J. P. Kotthaus, G. Weimann, and W. Schlapp, Phys. Rev. B **40**, 7874 (1989).

[13] A. Schenstrom, Y. J. Qian, M. F. Xu, H. P. Baum, M. Levy, and B. K. Sarma, Solid State Commun. **65**, 739 (1988).

[14] R. L. Willet, M. A. Paalanen, R. R. Ruel, K. W. West, L. N. Pfeiffer, and D. J. Bishop, Phys. Rev. Lett. **65**, 112 (1990).

[15] F. Guillion, A. Sachrajda, M. D'Iorio, R. Boulet, and P. Coleridge, Can. J. Phys. **69**, 461 (1991).

[16] J. M. Shilton, D. R. Mace, V. I. Talyanskii, Y. Galperin, M. Y. Simmons, M. Pepper, and D. A. Ritchie, J. Phys.: Condens. Matter **8**, L337 (1996).

[17] A. L. Fetter and J. D. Walecka, *Quantum Theory of Many-Particle Systems* (McGraw-Hill, New York, 1971).

[18] A. Knäbchen, Y. B. Levinson, and O. Entin-Wohlman, Phys. Rev. B, in press.

[19] S. H. Simon, preprint cond-mat/9605033 (1996).

[20] L. D. Landau and E. M. Lifschitz, *Electrodynamics of Continuous Media* (Pergamon, Oxford, 1984), Vol. 8.

[21] B. L. Altshuler and A. G. Aronov, in *Electron-Electron Interaction in Disordered Systems*, edited by A. L. Efros and M. Pollak (North-Holland, Oxford, 1985).

[22] D. Vollhardt and P. Wölfle, Phys. Rev. B **22**, 4666 (1980).

[23] E. Abrahams, P. W. Anderson, D. C. Licciardello, and T. V. Ramakrishnan, Phys. Rev. B **42**, 673 (1979).

[24] C. W. J. Beenakker and H. van Houten, in *Quantum Transport in Semiconductor Nanostructures*, Vol. 44 of *Solid State Physics*, edited by H. E. Ehrenreich and D. T. Turnbull (Academic Press, Boston, 1991).

[25] M. Born and E. Wolf, *Principles of Optics* (Pergamon, Oxford, 1975).

FIGURES

FIG. 1. Schematic drawing of the experiment. The quantum dot, shown in black, is of size L and is separated by a spacer layer of thickness d from the surface. The dielectric constants of the sample and the half-space above it are denoted by ϵ_0 and ϵ_1, respectively. The incoming and the transmitted waves have the wave vector $\boldsymbol{q}$, whereas $\boldsymbol{q'}$ is the wave vector of the scattered wave.

FIG. 2. Electron–surface-acoustic phonon interaction processes. The phonons are represented by wavy lines, and the electrons are depicted by straight lines. Diagram (a) shows the absorption of an incoming phonon (wave vector $\boldsymbol{q}$, energy $\boldsymbol{\omega}$). Diagrams (b) and (c) show scattering processes with two different intermediate states.

FIG. 3. Double logarithmic plot of the absorption and the scattering cross-sections as a function of the wave vector.

FIG. 4. Polar diagrams of the absorption cross-section $\eta_{abs}(\boldsymbol{q})$, Eq. (1), of a rectangular (main plot) and a square dot (inset). $\boldsymbol{\eta_{abs}(q)}$ [in $\boldsymbol{\mu}$m] is a function of the angle of incidence of the SAW and is given for three different wave numbers q.

FIG. 5. Polar diagram of the elastic scattering cross-section $\eta_{sc}(\boldsymbol{q'},\boldsymbol{q})$, Eq. (2), of a square dot. $\boldsymbol{\eta_{sc}}$ [in $\boldsymbol{\mu}$m] is considered as a function of the direction $\boldsymbol{q'}$ of the outgoing wave; the angle of incidence ($\boldsymbol{q}$) is kept fixed, see inset.

FIG. 6. Weak localization enhancement $1-\Re[\delta D]/D$, Eq. (60), of the absorption cross-section, Eq. (49), as a function of the magnetic field B for three different wave numbers.

Figure 1

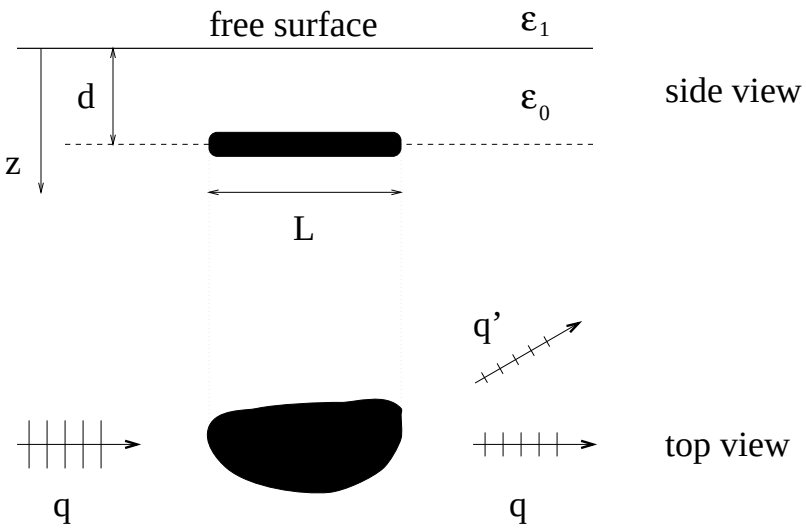

2a)

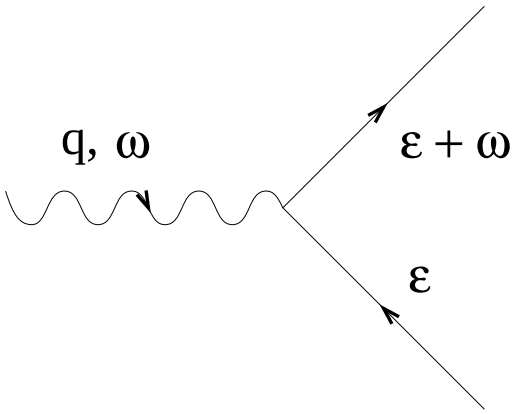

2b)

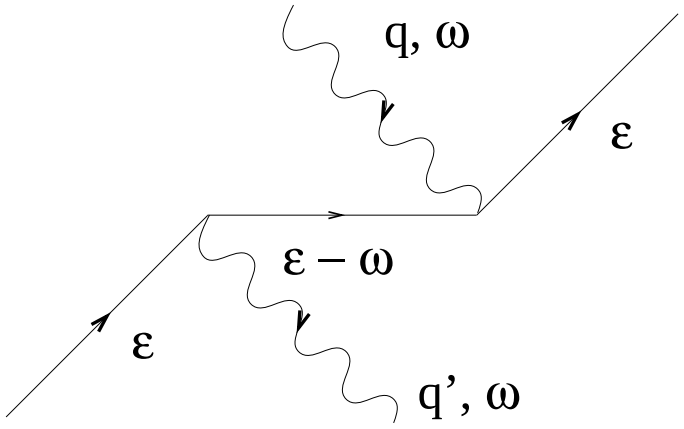

2c)

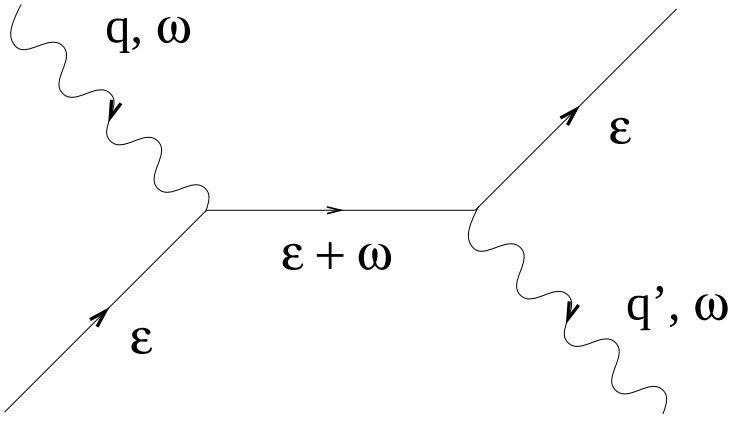

Figure 3

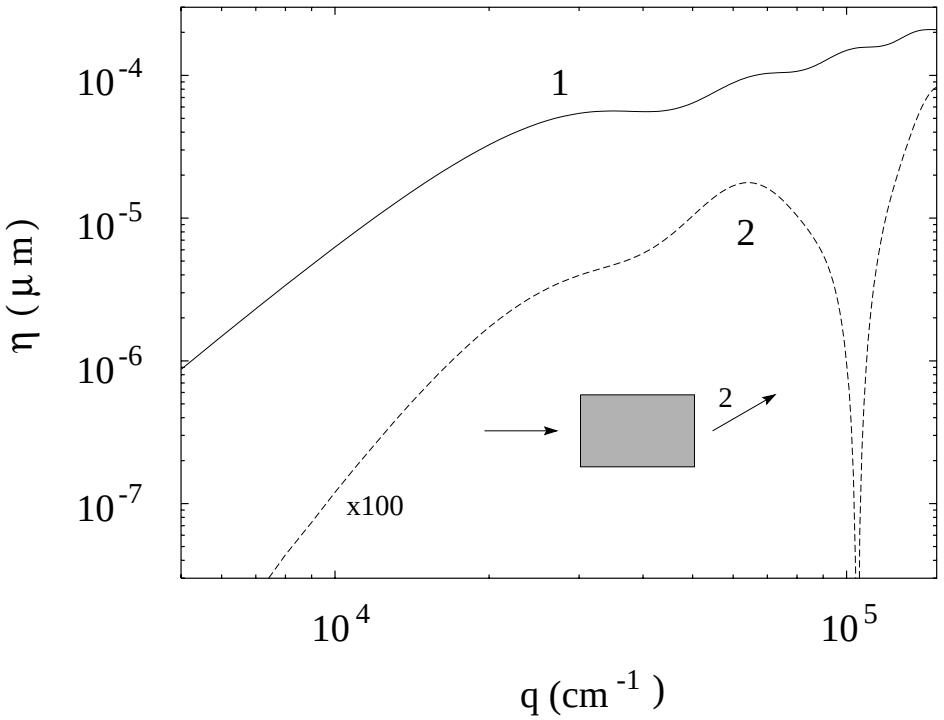

Figure 4

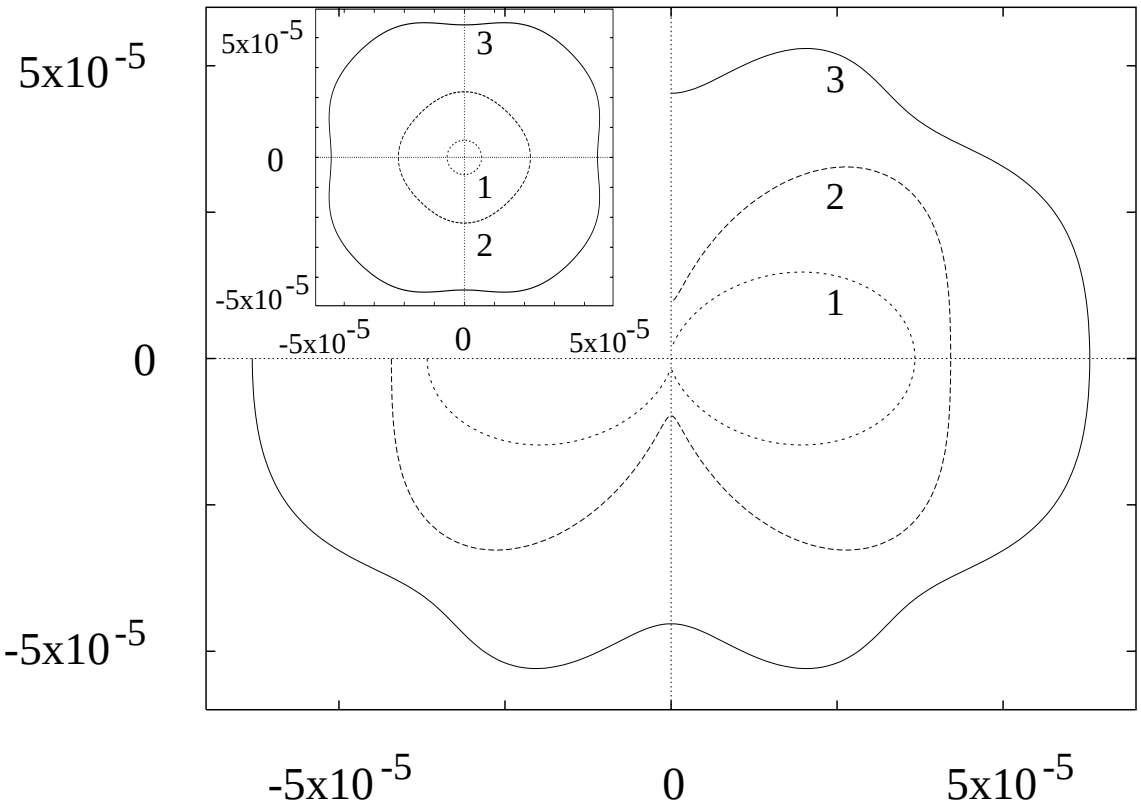
5x10-5
0
-5x10-5
-5x10-5
0
5x10-5
3
2
1
5x10-5
0
-5x10-5
-5x10-5
0
5x10-5
3
2
1

Figure 5

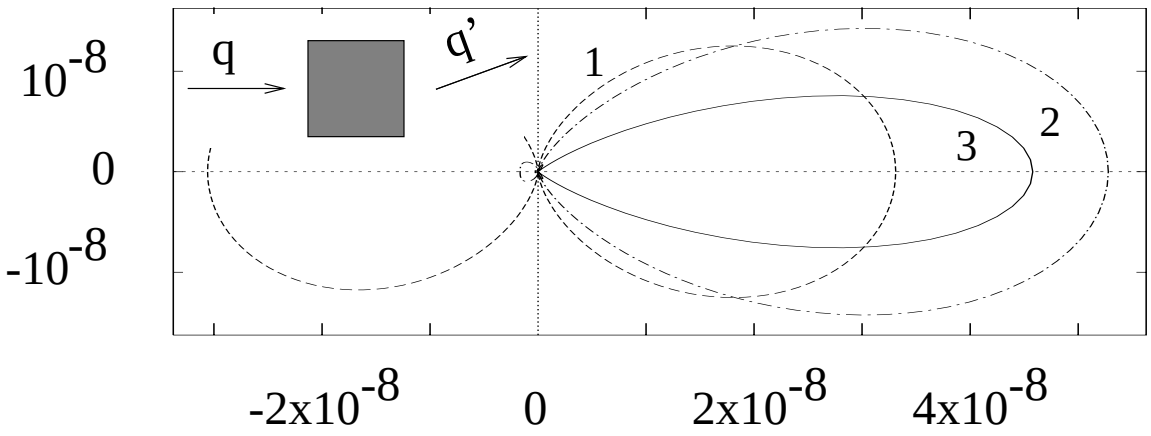

Figure 6

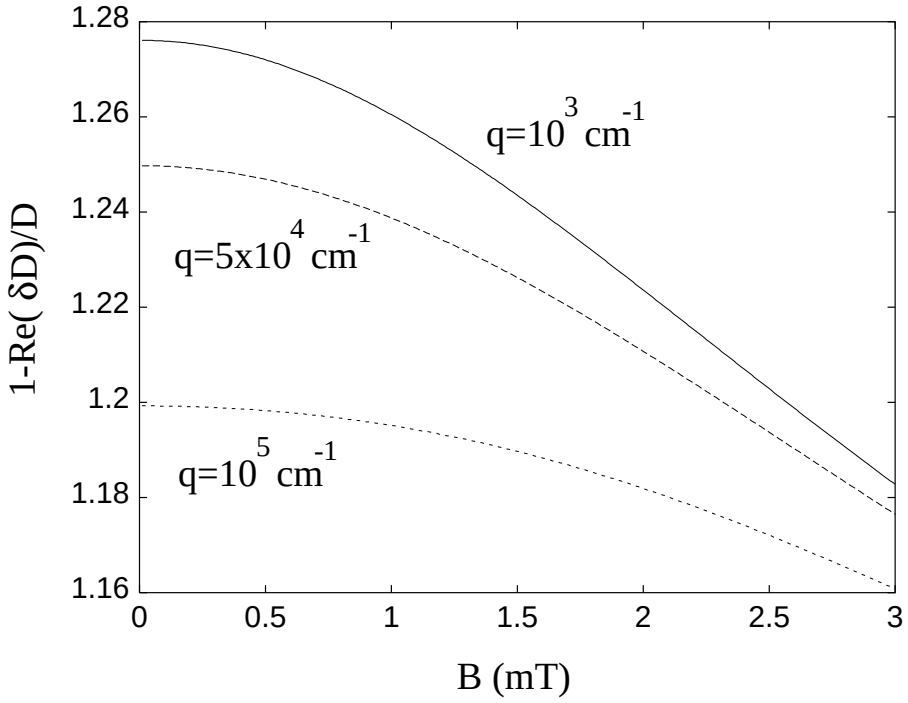
1.28
1.26
1.24
1.22
1.2
1.18
1.16
0
0.5
1
1.5
2
2.5
3
1-Re(δD)/D
B (mT)
q=10^3 cm^-1
q=5x10^4 cm^-1
q=10^5 cm^-1